

# Infinitely Deep Bayesian Neural Networks with Stochastic Differential Equations

**Winnie Xu**

University of Toronto, Vector Institute  
winniexu@cs.toronto.edu

**Ricky T.Q. Chen**

University of Toronto, Vector Institute  
rtqichen@cs.toronto.edu

**Xuechen Li**

Stanford University  
1xuechen@stanford.edu

**David Duvenaud**

University of Toronto, Vector Institute  
duvenaud@cs.toronto.edu

## Abstract

We perform scalable approximate inference in a continuous-depth Bayesian neural network family. In this model class, uncertainty about separate weights in each layer gives hidden units that follow a stochastic differential equation. We demonstrate gradient-based stochastic variational inference in this infinite-parameter setting, producing arbitrarily-flexible approximate posteriors. We also derive a novel gradient estimator that approaches zero variance as the approximate posterior over weights approaches the true posterior. This approach brings continuous-depth Bayesian neural nets to a competitive comparison against discrete-depth alternatives, while inheriting the memory-efficient training and tunable precision of Neural ODEs.

## 1 Introduction

Taking the limit of neural networks to be the composition of infinitely many residual layers provides a way to implicitly define its output as the solution to an ODE [18, 14]. This continuous-depth parameterization decouples the specification of the model from its computation. While the paradigm adds complexity, it has several benefits: (1) Computational cost can be traded for precision in a fine-grained manner by specifying error tolerances for adaptive computation, and (2) memory costs for training can be significantly reduced by running the dynamics backwards in time to reconstruct activations of intermediate states needed for backpropagation.

On the other hand, the Bayesian treatment for neural networks modifies the typical training pipeline such that instead of performing point estimates, a distribution over parameters is inferred. Although this approach adds complexity, it automatically accounts for model uncertainty – with which model averaging can be done to combat overfitting and improve calibration, especially on out-of-distribution data [53, 40].

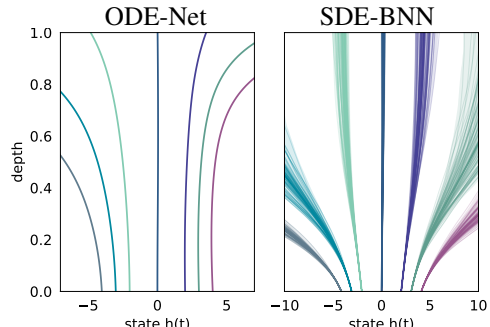


Figure 1: Hidden unit trajectories in an ODE-Net and an SDE-BNN. *Left:* A continuous-depth residual network has deterministic transformations of its hidden units from depths  $t = 0$  to  $t = 1$ . *Right:* Uncertainty in the weights of a Bayesian continuous-depth residual network implies uncertainty in its hidden unit activation trajectories. Shaded regions show densities over samples from the learned posterior dynamics. *Both:* Each distinct color corresponds to a different initial state corresponding to different data inputs.

How can we combine the benefits of continuous-depth models with those of Bayesian neural networks? The simplest approach is a “Bayesian neural ODE” [51, 7], which integrates out the finitely-many parameters of a standard neural ODE for prediction.

This approach is straightforward to implement, and can inherit the advantages of both Bayesian and continuous-depth neural nets. However, empirically, standard Gaussian approximate posteriors are a relatively poor match for neural ODEs, not to mention the drawbacks of also being used in the prior. Additionally, there is a special synergy available between continuous-time models and approximate inference that this approach does not exploit.

In this paper, we show that an alternative construction of Bayesian continuous-depth neural networks has additional practical benefits. Specifically, we consider the limit of infinite-depth Bayesian neural networks with separate unknown weights at each layer, a model class that we refer to as SDE-BNNs. We show that approximate inference can be done effectively using the scalable gradient-based variational inference scheme described by Li et al. [32], preliminary forms of which appeared in earlier works [1, 39, 47].

In this approach, the state of the output layer is computed by a black-box adaptive SDE solver, and the model is trained to maximize a variational lower bound. Figure 1 contrasts this neural SDE parameterization with the standard neural ODE approach. This approach maintains the adaptive computation and constant-memory cost of training Bayesian neural ODEs. In addition, it has two unique advantages:

- The variational posterior can be made arbitrarily expressive by simply enlarging the neural network that parameterizes the dynamics of the approximate posterior. Under mild conditions, this approach can approximate the true posterior arbitrarily closely.
- The variational objective admits a variance-reduced gradient estimator that is a natural extension of the “sticking the landing” trick [44]. Combined with arbitrarily expressive approximate posteriors, it is consistent and has vanishing variance as the approximate posterior approaches the true posterior.

Our low-variance gradient estimator can also be applied to variational inference in SDEs more generally, such as for time-series modeling, but such applications are beyond the scope of this paper.

## 2 Background

**Bayesian Neural Networks** Given a dataset, there are usually many functions that fit the data well, which a given neural network can express with different parameter values. Instead of making point estimates of the parameters, the Bayesian paradigm frames learning as posterior inference. Predictions are obtained through integration over many possible parameter settings. Formally, given a dataset  $\mathcal{D} = \{(x_i, y_i)\}_{i=1}^N$  and prior distribution over model weights  $p(w)$ , we want to compute the posterior  $p(w|\mathcal{D}) \propto p(\mathcal{D}|w)p(w)$ . This can be done by optimizing an approximate posterior distribution  $q(w)$  that minimizes the Kullback-Leibler (KL) divergence, i.e. maximizing the Evidence Lower Bound (ELBO):

$$\mathcal{L}_{\text{ELBO}}(\phi) = \mathbb{E}_{q(w)} [\log p(\mathcal{D}|w)] - D_{\text{KL}}(q(w)||p(w)). \quad (1)$$

Estimating gradients of this objective using simple Monte Carlo is known as stochastic variational inference (SVI) [21, 43]. One of the main technical challenges of SVI is choosing a parametric family of approximate posteriors that is tractable to sample from and evaluate, while being flexible enough to approximate the true posterior well. Most scalable inference techniques use Gaussian approximate posteriors with restricted covariance structure between the weights in the network [15, 3, 53, 36]. Others construct complex approximate posteriors using normalizing flows [31, 35] or through distillation [2, 49].

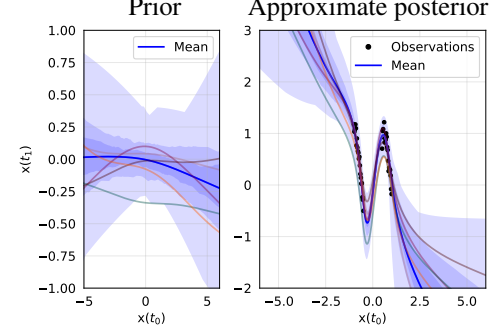


Figure 2: Predictive prior and posterior of the SDE-BNN on a non-monotonic toy dataset. Blue areas indicate density percentiles, and distinct colored lines show model samples.

**Neural Ordinary Differential Equations** Neural ordinary differential equations [6] define ODEs using neural networks:

$$dh_t = f_\theta(h_t, t) dt, \quad h_0 \in \mathbb{R}^d, \quad (2)$$

where  $f : \mathbb{R}^d \times \mathbb{R} \rightarrow \mathbb{R}^d$  is a Lipschitz function defined by a neural network with parameters  $\theta$ . Starting at an initial value  $h_0 = x$  given by a data example and integrating these dynamics forward for a finite time can be seen as passing the input through an infinitely-deep residual network. For learning scalar-valued functions, if extra dimensions are added to  $h$ , and the network is capped with a linear layer at the end, then these networks have similar universal approximation properties as standard neural networks [11, 55], and can be trained by standard stochastic gradient descent methods. Using adaptive ODE solvers allows one to trade evaluation speed for precision. The adjoint sensitivity method also saves memory during training through reconstructing the trajectory of the hidden units  $h$  by running the dynamics backwards during backpropagation.

## 2.1 Latent Stochastic Differential Equations

Informally, an SDE can be viewed as an ODE with infinitesimal noise added throughout time. It typically takes the following form:

$$dw_t = f_\theta(w_t, t) dt + g_\theta(w_t, t) dB_t, \quad (3)$$

where  $w_0 \in \mathbb{R}^d$  is the initial state,  $f_\theta : \mathbb{R}^d \times \mathbb{R} \rightarrow \mathbb{R}^d$  and  $g_\theta : \mathbb{R}^d \times \mathbb{R} \rightarrow \mathbb{R}^{d \times m}$  are functions Lipschitz in both arguments, dubbed the *drift* and *diffusion*, respectively, and  $\{B_t\}$  is an  $m$ -dimensional Brownian motion.

Some works has considered training SDEs with dynamics parameterized by neural networks [32, 47, 42, 22, 29, 33]. Note that directly optimizing the drift and diffusion functions to maximize the average log-likelihood of an observation  $\log p(y_t|w_t)$  would result in the diffusion approaching 0, conditional on the ODE fitting the training data well with the diffusion somewhat unconstrained.

Instead of directly optimizing the parameters of an SDE to match the data, a better approach is to use an SDE to define a prior over trajectories of  $w$ , and optimize the marginal likelihood of the data, integrating over all trajectories of  $w$  weighted by the prior. Luckily, we can specify an approximate posterior over trajectories using a second SDE. We define the approximate posterior by

$$dw_t = f_\phi(w_t, t) dt + g_\theta(w_t, t) dB_t. \quad (4)$$

When the dynamics function of the approximate posterior  $f_\phi$  is parameterized by a neural network, this family of approximate posteriors is extremely expressive. For example, Figure 3 shows that such a variational family can easily approximate non-Gaussian and multi-modal posteriors on path space.

If both the SDE defined on equation 3 and equation 4 share the same diffusion function, then the KL between the two induced measures on path space has the following form [32, 47]:

$$D_{\text{KL}}(\mu_q || \mu_p) = \mathbb{E}_{q_\phi(w)} \left[ \int_0^1 \frac{1}{2} \|u(t, \phi)\|_2^2 dt \right] \quad (5)$$

$$\text{where } u(t, \phi) = g_\theta(w_t, t)^{-1} [f_\theta(w_t, t) - f_\phi(w_t, t)] \quad (6)$$

,  $\mu_q$  and  $\mu_p$  are path space probability measures induced respectively by equation 4 and equation 3, and the expectation is taken under the approximate posterior process, denoted  $q_\phi(w)$ . Intuitively, this KL divergence resembles the summative difference over time horizon  $[0, 1]$  between the prior drift  $f_\theta$  and the  $f_\phi$ , scaled by the diffusion. This divergence can be estimated up to a constant with simple Monte Carlo, sampling trajectories from the dynamics given by the approximate posterior.

**SDEs can represent arbitrarily expressive approximate posteriors** To ensure that the KL divergence between the prior and approximate posterior on path space is finite, one must use exactly the same diffusion function  $g_\theta(w_t, t)$  for the approximate posterior and the prior. Surprisingly, this does

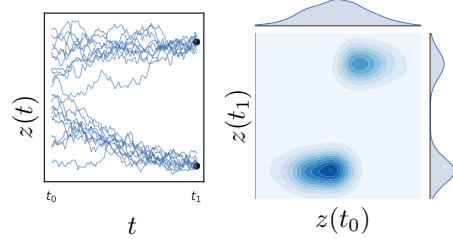


Figure 3: Neural SDEs can learn arbitrarily expressive approximate posteriors. *Left:* Samples from an approximate posterior, trained with an OU prior and conditioned on two observations with Cauchy likelihoods. *Right:* Joint distribution and marginals of the approximate posterior process  $z$  at times  $t_0$  and  $t_1$ .

not limit the expressivity of the approximate posterior. Boué et al. [4] show that there is a one-to-one correspondence between the space of path measures and drift functions that result in the same path space KL divergence. This implies that any path space measure close to the true posterior can be instantiated by SDEs with appropriate drifts. It follows that an approximate posterior parameterized by a sufficiently expressive family of function approximators can be made arbitrarily close to the true posterior. Similarly, Tzen and Raginsky [47, Section 4], using the fact derived from Boué, characterize the Girsanov reparameterization of the variational formula, where the evidence lower bound is tight when the drift is optimal.

### 3 Infinitely Deep Bayesian Neural Nets

Standard discrete-depth residual networks can be defined as a composition of layers of the form:

$$h_{t+\epsilon} = h_t + \epsilon f(h_t, w_t), \quad t = 1 \dots T, \quad (7)$$

where  $t$  is the layer index,  $h_t \in \mathbb{R}^{D_h}$  denotes a vector of hidden unit activations at layer  $t$ , the input  $h_0 = x$ , and  $w_t \in \mathbb{R}^{D_w}$  represents the parameters for layer  $t$ . In the discrete setting,  $\epsilon = 1, \in \mathbb{R}$ .

We can construct a continuous-depth variant of residual networks by setting  $\epsilon = 1/T$  and taking the limit as  $T \rightarrow \infty$ . This yields a differential equation that describes the hidden unit evolution as a function of depth  $t$ . Since standard residual networks are parameterized with different “weights” per layer, we denote the weights at layer  $t$  by  $w_t$ . To specify different weights at each layer with a finite number of parameters, we can introduce a hypernetwork  $f_w$  that specifies the change in weights as a function of depth and the current weights [17]. The evolution of the hidden unit activations and weights can then be combined into a single differential equation:

$$\frac{d}{dt} \begin{bmatrix} h_t \\ w_t \end{bmatrix} = \begin{bmatrix} f_h(t, h_t, w_t) \\ f_w(t, w_t) \end{bmatrix} \quad (8)$$

with some learned initial weight value  $w_{t_0}$ . Using time-varying weights is similar to augmenting the state [11, 56]. See Appendix Figure 8 for details on the effects of augmentation. We then perform Bayesian inference on the weight process  $w_t$ , assigning a suitable prior stochastic process and performing variational inference in this infinitesimal limit.

Like all Bayesian neural networks with observation likelihoods, our framework models uncertainty both about parameters and about individual observations: The likelihood  $p(y|h_1)$  captures the noise in observations, while the SDE encodes uncertainty about the weights.

**Prior process on weights** Typical priors for Bayesian neural networks use independent Gaussians across all weights and layers. Taking the infinitesimal limit of such a prior would give a white noise process prior on the weights  $w(\cdot)$ . However, scaling this noise to result in finite variance is difficult [41, 42].

Instead, we use the Ornstein–Uhlenbeck (OU) process as the prior on weights. The process is characterized by an SDE with drift and diffusion:

$$f_p(w_t, t) = -w_t, \quad g(w_t, t) = \sigma I_d, \quad (9)$$

respectively, where  $\sigma$  is a hyperparameter. We choose this prior due to its simplicity and because its marginal variance approaches a constant in the large time limit, remaining bounded.

**Approximate posterior over weights** We parameterize the approximate posterior on weights implicitly using another SDE with the following drift function:

$$f_q(w_t, t, \phi) = \text{NN}_\phi(w_t, t, \phi) - f_p(w_t, t). \quad (10)$$

This drift function  $f_q$  is parameterized by a small neural network (NN) with parameters  $\phi$ . With this drift, the approximate posterior process will in general have non-Gaussian, non-factorized marginals, and its expressive capacity can be increased by making the neural net larger.

**Evaluating the network** Evaluating our network at a given input requires marginalizing over weight and hidden unit trajectories. This can be done with simple Monte Carlo, sampling a weight path  $\{w_t\}$  from the posterior process and evaluating the network activations  $\{h_t\}$  given the sampled

weights and the input. Both steps require solving a differential equation. Luckily, both steps can be done simultaneously by a single SDE solver call with the augmented state SDE:

$$d \begin{bmatrix} w_t \\ h_t \end{bmatrix} = \begin{bmatrix} f_w(w_t, t, \phi) \\ f_h(h_t, t, w_t) \end{bmatrix} dt + \begin{bmatrix} g_w(w_t, t) \\ \mathbf{0} \end{bmatrix} dB_t, \quad (11)$$

where  $h_0 = x$ , the input. The learnable parameters are the initial weight values at time zero  $w_0$  (either point estimated or inferred) and those of the drift function  $\phi$ .

**Output likelihood** The final state of the hidden units  $h_1$  is used to parameterize the likelihood of the target output  $y$ :  $\log p(y|x, w) = \log p(y|h_1)$ . For instance,  $p(y|h_1)$  could be a Cauchy likelihood for regression, or categorical likelihood for classification.

**Training objective** To fit the network to data, we maximize the lower bound on marginal likelihood given by the infinite-dimensional ELBO:

$$\mathcal{L}_{\text{ELBO}_\infty}(\phi) = \mathbb{E}_{q_\phi(w)} \left[ \log p(\mathcal{D}|w) - \int_0^1 \frac{1}{2} \|u(w_t, t, \phi)\|_2^2 dt \right].$$

The sampled weights, the hidden activations, and the training objective are all computed simultaneously with a single call to an adaptive SDE solver. Gradients of the sampled loss can also be efficiently computed using adaptive solvers, following Li et al. [32].

## 4 Variance-Reduced Gradient Estimation

Roeder et al. [44] showed that when optimizing expectations using the reparameterization gradient, a gradient estimator with lower variance can be constructed by removing a score function term that has zero expectation, and that the variance of this gradient estimator approaches zero as the approximate posterior approaches the true posterior. We refer to this general trick as “sticking the landing” (STL). We adapt this idea to the SDE setting by replacing the original estimator of the path space KL with the following STL estimator:

$$\widehat{\text{KL}}_{\text{STL}} = \int_0^1 \frac{1}{2} \|u(w_t, t, \phi)\|_2^2 dt + \int_0^1 u(w_t, t, \perp(\phi)) dB_t, \quad w(\cdot) \sim q_\phi(w) \quad (12)$$

where  $u$  is defined in equation 6, the path  $\{w_t\}_{t \in [0, T]}$  is sampled from the approximate posterior process, and  $\perp(\cdot)$  is the stop gradient function that renders the input a constant with respect to which gradient propagation is stopped.

The second term in equation 12 is a martingale and has expectation zero. Therefore, in prior works [32, 47, 48], Monte Carlo estimation was only performed for the first term, but we find that this approach does not necessarily reduce the variance of the gradient (Figure 4).

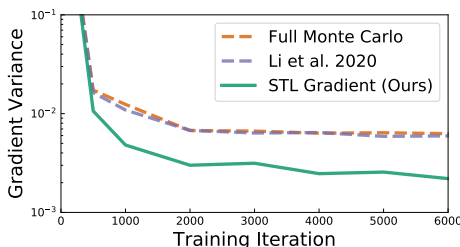


Figure 4: Comparison of the variance in three gradient estimators. On this toy problem, our new gradient estimator reduces variance by a factor of roughly 4.

Because our approximate posterior can be made arbitrarily expressive, we conjecture that our approach can achieve arbitrarily low gradient variance towards the end of training if the network parameterizing  $f_w$  is made expressive enough. See Appendix is A.2 for a heuristic derivation.

We show the variance of different gradient estimators in Figure 4, averaged across the parameters  $\theta$ , in a 1D regression setting. We compare STL against a “Full Monte Carlo” estimate which includes the second additional term without gradient stopping, as well as the estimator that was previously used by Li et al. [32] which ignores the second term. Figure 4 shows that STL obtains lower variance than alternatives, when matching an exponentiated Brownian motion. Table 4 shows training performance improvements.

Table 1: Classification accuracy and expected calibration error (ECE) on MNIST and CIFAR-10. We separate models into point estimates, discrete-time models, and continuous-time models. Our SDE-BNN approach outperforms other continuous-time Bayesian neural nets and brings them into competitive performance against discrete-time Bayesian neural nets. <sup>†</sup>Results reported by Izmailov et al. [24] where a modified residual network architecture was used; only one seed was reported.

| Model                              | MNIST            |                          | CIFAR-10         |                          |
|------------------------------------|------------------|--------------------------|------------------|--------------------------|
|                                    | Accuracy (%)     | ECE ( $\times 10^{-2}$ ) | Accuracy (%)     | ECE ( $\times 10^{-2}$ ) |
| ResNet32                           | 99.46 $\pm$ 0.00 | 2.88 $\pm$ 0.94          | 87.35 $\pm$ 0.00 | 8.47 $\pm$ 0.39          |
| ODEnet                             | 98.90 $\pm$ 0.04 | 1.11 $\pm$ 0.10          | 88.30 $\pm$ 0.29 | 8.71 $\pm$ 0.21          |
| HyperODEnet                        | 99.04 $\pm$ 0.00 | 1.04 $\pm$ 0.09          | 87.92 $\pm$ 0.46 | 15.86 $\pm$ 1.25         |
| MFVI ResNet32                      | 99.44 $\pm$ 0.00 | 2.76 $\pm$ 1.28          | 86.97 $\pm$ 0.00 | 3.04 $\pm$ 0.94          |
| MFVI <sup>†</sup>                  | —                | —                        | 86.48            | 1.95                     |
| Deep Ensemble <sup>†</sup>         | —                | —                        | 89.22            | 2.79                     |
| HMC (“gold standard”) <sup>†</sup> | 98.31            | 1.79                     | 90.70            | 5.94                     |
| MFVI ODEnet                        | 98.81 $\pm$ 0.00 | 2.63 $\pm$ 0.31          | 81.59 $\pm$ 0.01 | 3.62 $\pm$ 0.40          |
| MFVI HyperODEnet                   | 98.77 $\pm$ 0.01 | 2.82 $\pm$ 1.34          | 80.62 $\pm$ 0.00 | 4.29 $\pm$ 1.10          |
| SDE BNN                            | 99.30 $\pm$ 0.09 | 0.63 $\pm$ 0.10          | 89.84 $\pm$ 0.94 | 7.19 $\pm$ 0.37          |
| SDE BNN (+ STL)                    | 99.10 $\pm$ 0.09 | 0.78 $\pm$ 0.12          | 89.10 $\pm$ 0.45 | 7.97 $\pm$ 0.51          |

## 5 Experiments

As a proof of concept for this class of continuous-depth parameterizations, we investigate the effectiveness of our proposed approximate inference method for training continuous-depth neural nets, referred to as SDE-BNN, in terms of classification accuracy, calibration, perturbation robustness, and speed-precision trade-offs. Our code is publicly available [here](#). Experimental settings in Table 2.

We consider toy regression tasks and image classification tasks on MNIST and CIFAR-10. We also investigate out-of-distribution generalization. Notably, our approach does not require *post hoc* recalibration methods such as training with temperature scaling [16] or isotonic regression [52].

**Backpropagation through solvers vs. adjoint** We experimented with fixed- and adaptive-step SDE solvers, as well as the stochastic adjoint of Li et al. [32]. Figure 5 shows similar convergence for both approaches. Appendix A.3 shows that both approaches used similar numbers of dynamics function evaluations, and also shared similar wall-clock time.

The overhead for estimating error in our adaptive solvers was substantial; therefore, for final model evaluation, we trained with fixed-step solvers, where the number of steps is chosen to be large enough to match the convergence speed of our adaptive-step solvers.

**Baselines** For a fixed-depth network baseline, we compare to standard residual networks. We then test variational inference on the weights of these residual network architectures.

We also perform ablation studies to compare ours to more standard variational inference approaches over continuous-depth networks. Specifically, we compare to a mean field variational inference (MFVI) ODEnet where stochastic variational inference is performed over weights that do not vary across depth. This baseline is a fully-factorized Gaussian approximate posterior, *i.e.* mean-field approximation, and been used for Neural ODEs by Look and Kandemir [34], Dandekar et al. [7].

We further compare our model to a MFVI HyperODEnet, where a learned drift is applied to  $w$ , but mean-field inference is instead performed over the parameters of the hypernetwork. Alternatively, one can interpret this as another MFVI ODEnet with a larger state and a more complex drift function but that has similar computational complexity as our SDE-BNN approach. This setting stands in contrast to our approach where Bayesian inference is carried out over the entire continuous-depth network as a stochastic process.

**Parameterizing the drift function** We parameterized the drift function of the variational posterior  $f_w$  using a simple multilayer perceptron. To ensure optimization starts at a stable set of dynamics, we

also subtract the prior drift so that when the final layer is initialized to output zero, the approximate posterior equals the prior.

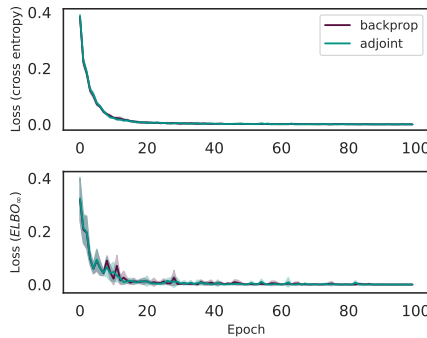


Figure 5: Benchmarking two gradient computation methods: (1) Back-propagation through the SDE solver, and (2) the memory-efficient stochastic adjoint of Li et al. [32]. Both methods have similar optimization dynamics, final performance, and wall-clock time, but the adjoint approach is more memory-efficient. Detailed comparisons of wall-clock time and evaluation step results in Appendix A.3.5.

because the hidden states  $h$  do not receive additive instantaneous noise. Only on the weights  $w$  do we apply instantaneous noise.

## 5.2 Image Classification

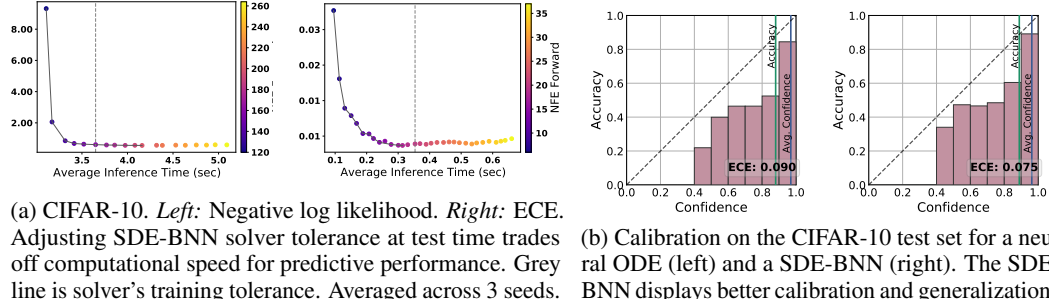


Figure 6: Performance of SDE-BNN on standard CIFAR-10 classification task.

Instantaneous changes to the hidden state ( $f_h$ ) are parameterized using a convolutional neural network, including one strided convolution for downsampling and a transposed convolution layer for upsampling. We then set the weights  $w$  to be the filters and biases of all the convolutional layers. The approximate posterior drift dynamics ( $f_w$ ) is a multilayer perceptron with hidden layer widths of 2, 128, and 2. The small hidden width of the bottleneck layers was chosen to reduce the number of variational parameters and promote linear scaling with respect to the dimension of  $w$ . On MNIST, we used one such SDE-BNN block, while on CIFAR-10, we used a multi-scale variant where multiple SDE-BNN blocks were stacked with the invertible downsampling from Dinh et al. [10] in between.

We report classification results in Table 1. The SDE-BNN generally outperforms the baselines, and we notice that while the continuous-depth Neural ODE (ODEnet) models can achieve similar classification performance on a standard residual network, it consistently has poorer calibration.

The SDE-BNN matches and outperforms the accuracy of standard residual networks on MNIST and CIFAR-10, respectively, while obtaining lower expected calibration errors (ECE). From ablation studies, we found that it was harder to achieve similar performance with either of the mean field

variants of an ODEnet, and that they demonstrated a worse trade-off between performance and calibration.

Figure 6a demonstrates the ability of SDE-BNNs, like neural ODEs before them, to trade off computation time for precision. Figure 12 in Appendix A.3.2 indicates that calibration is insensitive to solver tolerances close to the value used during training.

### 5.2.1 Calibration

Table 1 quantifies our model’s calibration with expected calibration error (ECE; Guo et al. [16]). The SDE-BNN appears better calibrated than the Neural ODE [6] and mean field ResNet baselines. Figure 6b shows better calibration than neural ODEs with similar accuracy. Appendix Figure 11 shows the insensitivity of these results to solver step size.

### 5.2.2 Robustness to Input Corruption

We show the robustness of SDE-BNNs by evaluating on all 19 non-adversarial corruptions across 5 severity levels in the CIFAR10-C [20] benchmark. These corruptions mimic real-world perturbations such as noise, blur, and weather. To evaluate the classification robustness of the SDE-BNN, we compare the mean corruption error (mCE), the average error for each intensity level summed across all 19 perturbations, to the top-1 error rate on the corresponding clean CIFAR-10 dataset.

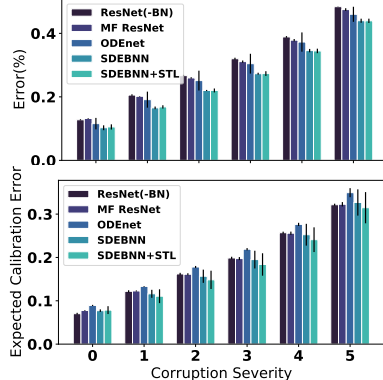


Figure 7: CIFAR10-C. Robustness to distributional shifts on CIFAR-10. SDE-based neural nets show better accuracy and calibration than non-Bayesian and mean-field methods. Black bars show standard deviation over 3 seeds.

Figure 7 shows error on the corrupted test set relative to uncorrupted data, demonstrating a steady increase in mCE across increasing perturbation severity levels along with the overall error measurement summarized in Table 1. On both CIFAR-10 and CIFAR10-C, the SDE-BNN and SDE-BNN + STL models achieve lower overall test error and better calibration than the baselines.

Compared to the standard baselines (ResNet32 and Mean Field (MF) ResNet32), SDE-BNN achieves around 4.4% lower absolute corruption error (CE), the total classification error for all corruption tasks across all 5 severity levels [20], in comparison to the clean errors. The effectiveness of learned uncertainty on out-of-domain inputs indicates that SDE-BNN is more robust to observation perturbations despite not being trained on such diverse forms of corruptions.

## 6 Scope and Limitations

**Computational speed** The cost of evaluating our model grows in  $\mathcal{O}(DT)$ , where  $D$  is the number of weights, and  $T$  the number of iterations taken by the solver. This may seem advantageous compared to the  $\mathcal{O}(D^3)$  cost for non-factorized Gaussian approximate posteriors, but the number of steps required is difficult to characterize. Although our approach allows adjustment of the computational cost at test time, it is harder to control the cost of evaluation during training time, making our method relatively slow to train. However, it should be straightforward to regularize these models to be faster to solve, as in Kelly et al. [25]. Relatedly, Dusenberry et al. [12] recently demonstrated an  $\mathcal{O}(DK)$  cost approximate posterior in standard BNNs.

**Batch norm** We did not incorporate batch normalization [23] in any of our neural network components. Introducing any normalization (e.g. batchnorm, layernorm, etc.) compromises the Lipschitz property required for SDEs to have a unique solution. Since BN introduces dependence between samples within a batch, it is also unclear how to incorporate BN while maintaining the consistency properties of Bayesian inference. Zhang et al. [54], Chang et al. [5] proposed initializations that yield the same performance without needing batch normalization.

**Low-variance gradients for other domains** Our extention of the STL gradient estimator [44] to the infinite-dimensional variational objective could also be used in other settings for faster convergence, such as the time series applications Li et al. [32] investigated.

## 7 Related Work

**Initial theoretical investigations** The earliest theoretical treatment of infinitely-deep Bayesian neural networks was made by Neal [37, Chapter 2], but no practical training or evaluation method was proposed. Duvenaud et al. [13] also investigated the theoretical properties of kernel-based constructions of infinitely-deep Bayesian neural networks.

**Diffusion limits of discrete-time models** We expect existing discrete-depth constructions to converge to diffusion limits in the infinitesimal limit if a system is updated with appropriately scaled Gaussian noise at each timestep. Peluchetti and Favaro [42, 41] show this holds for the output of residual networks with shallow residual blocks whose weight initializations are appropriately scaled. While our construction of the SDE-BNN model given by equation 11 seems similar to that suggested in [42], we comment on two key differences: (i) We strictly enforce hidden states to follow a diffusion throughout training, whereas Peluchetti and Favaro [42] only ensures this at initialization, and (ii) we adopt a more general neural net architecture for the residual blocks and than the shallow ones considered in [42]. The consequence of (i) is that operations on diffusions (e.g., computing path-space KL) remain applicable even after our model has been trained. While (ii) appears to be a minor difference, it actually uncovers a fundamental distinction in our analysis: Since we start out with an SDE, and only discretize for numerical computations, our model is able to incorporate any type of Lipschitz smooth residual block. The analysis by Peluchetti and Favaro [42], which relies on Taylor expanding the residual block function, is not straightforward in the presence of complex residual block architectures and would require modifications to the initialization.

Tzen and Raginsky [47] show that particle trajectories of the approximate posterior in discrete deep latent Gaussian models converge to a diffusion, and that the ELBO may be written down using the KL of measures on path space. We note that this construction has been explored in various forms in the past [39, 1], with a more general formulation encapsulating non-constant diffusions and practical implementation applied to time series data by Li et al. [32].

**Neural SDEs with other training objectives** Models making use of SDEs have appeared in the past, though many make use of somewhat *ad-hoc* combinations of methods involving both discrete and continuous components. Kong et al. [29] proposed fitting a neural SDE by using a heuristic training objective based on encouraging the diffusion to be large away from the training data and a fixed Euler-Maruyama (E-M) discretization. Innes et al. [22] trained neural SDEs by backpropagating through the operations of the solver, however their training objective simply matched the first two moments of the training data, implying that it could not consistently estimate diffusion functions. This approach is also relatively memory-intensive. Liu et al. [33] and Oganesyan et al. [38] add noise to the solver operations in a neural ODE, although the diffusion must be tuned as a hyperparameter. Hegde et al. [19] proposed a form of neural SDE using Gaussian processes to parameterize the drift and diffusion functions for a fixed E-M discretization. However, the diffusion functions are based on an *ad-hoc* construction from a Gaussian process posterior conditioned on inducing points. Ryder et al. [46] used a Gaussian process variational posterior, effectively a continuous-time analog of a mean field approximation that may not always be expressive enough to model the true posterior. Kidger et al. [26] learn neural SDEs by jointly learning a discriminator [27] and formalize the problem as learning generative adversarial networks. However, this would involve many more hyperparameters and require extensive tuning compared to our variational inference approach.

**Neural ODEs with finite-dimensional stochasticity** Some methods based on building variational autoencoders with a neural ODE share similar training objectives, since the ELBO appears frequently in posterior inference. The Latent ODE model [45] only performs inference on the distribution at an initial time of a continuous hidden state. De Brouwer et al. [8] introduced stochastic jumps at data locations, and do not perform continuous-time inference. While performing amortized inference for time series modeling, Yıldız et al. [51] also infer the weights of an ODE drift function. Dandekar et al. [7] have a similar setting but for supervised learning.

**Approximate posteriors defined with neural nets** Krueger et al. [31] and Louizos and Welling [35] use normalizing flows to construct a non-factorized, non-Gaussian approximate posterior in Bayesian neural networks. However, normalizing flows have poor scaling with dimension and point estimates were used for most of the weights in the neural network. Table 5 in Appendix 5 compares qualities of our approach to existing methods for stochastic variational inference in BNNs.

## 8 Conclusion

We developed a practical method for approximate inference in continuous-depth Bayesian neural networks. Our approach exploits a special synergy between continuous-depth models and variational inference for SDEs, providing additional benefits over standard approaches. In particular, our method allows arbitrarily-expressive, non-factorized approximate posteriors implicitly defined through neural SDEs. We also developed an unbiased gradient estimator for SDE variational inference whose variance approaches zero as the approximate posterior approaches the true posterior. This combination gives our family of Bayesian continuous-depth neural networks a special property, which is that the gradients’ bias and variance can be made arbitrarily small during training. Where standard applications of MFVI on continuous-depth models perform poorly, our approach brings continuous-depth Bayesian neural networks to a comparable performance with standard Bayesian neural networks.

## 9 Broader Impact

We expect the main impact of this work to be towards the improvement of models with better calibration and predictive uncertainties that would be conducive to better signals regardless of the domain of application in which they are used. The societal impacts aside from the general of deep learning approaches and ethical concerns of neural networks are not immediately foreseeable.

## References

- [1] Archambeau, C., Opper, M., Shen, Y., Cornford, D., and Shawe-Taylor, J. (2008). Variational inference for diffusion processes. *Advances in Neural Information Processing Systems*.
- [2] Balan, A. K., Rathod, V., Murphy, K. P., and Welling, M. (2015). Bayesian dark knowledge. In *Advances in Neural Information Processing Systems*, pages 3438–3446.
- [3] Blundell, C., Cornebise, J., Kavukcuoglu, K., and Wierstra, D. (2015). Weight uncertainty in neural networks. *arXiv preprint arXiv:1505.05424*.
- [4] Boué, M., Dupuis, P., et al. (1998). A variational representation for certain functionals of brownian motion. *The Annals of Probability*, 26(4):1641–1659.
- [5] Chang, O., Flokas, L., and Lipson, H. (2020). Principled weight initialization for hypernetworks. In *ICLR*.
- [6] Chen, R. T. Q., Rubanova, Y., Bettencourt, J., and Duvenaud, D. (2018). Neural ordinary differential equations. *Advances in Neural Information Processing Systems*.
- [7] Dandekar, R., Dixit, V., Tarek, M., Garcia-Valadez, A., and Rackauckas, C. (2020). Bayesian neural ordinary differential equations. *arXiv preprint arXiv:2012.07244*.
- [8] De Brouwer, E., Simm, J., Arany, A., and Moreau, Y. (2019). Gru-ode-bayes: Continuous modeling of sporadically-observed time series. *arXiv preprint arXiv:1905.12374*.
- [9] Deng, L. (2012). The mnist database of handwritten digit images for machine learning research. *IEEE Signal Processing Magazine*, 29(6):141–142.
- [10] Dinh, L., Sohl-Dickstein, J., and Bengio, S. (2016). Density estimation using real nvp. *arXiv preprint arXiv:1605.08803*.
- [11] Dupont, E., Doucet, A., and Teh, Y. W. (2019). Augmented neural odes. In *NeurIPS*.
- [12] Dusenberry, M., Jerfel, G., Wen, Y., Ma, Y., Snoek, J., Heller, K., Lakshminarayanan, B., and Tran, D. (2020). Efficient and scalable bayesian neural nets with rank-1 factors. In *International conference on machine learning*, pages 2782–2792. PMLR.
- [13] Duvenaud, D., Rippel, O., Adams, R. P., and Ghahramani, Z. (2014). Avoiding pathologies in very deep networks. In *Artificial Intelligence and Statistics*.
- [14] E, W. (2017). A Proposal on Machine Learning via Dynamical Systems. *Commun. Math. Stat.*, 5(1):1–11.
- [15] Graves, A. (2011). Practical variational inference for neural networks. In *Advances in neural information processing systems*, pages 2348–2356.
- [16] Guo, C., Pleiss, G., Sun, Y., and Weinberger, K. Q. (2017). On calibration of modern neural networks. In *Proceedings of the 34th International Conference on Machine Learning-Volume 70*, pages 1321–1330. JMLR. org.
- [17] Ha, D., Dai, A., and Le, Q. V. (2016). Hypernetworks. *arXiv preprint arXiv:1609.09106*.
- [18] Haber, E. and Ruthotto, L. (2017). Stable architectures for deep neural networks. *Inverse Problems*, 34(1):014004.
- [19] Hegde, P., Heinonen, M., Lähdesmäki, H., and Kaski, S. (2018). Deep learning with differential gaussian process flows. *arXiv preprint arXiv:1810.04066*.
- [20] Hendrycks, D. and Dietterich, T. (2019). Benchmarking neural network robustness to common corruptions and perturbations. *Proceedings of the International Conference on Learning Representations*.
- [21] Hoffman, M. D., Blei, D. M., Wang, C., and Paisley, J. (2013). Stochastic variational inference. *The Journal of Machine Learning Research*, 14(1):1303–1347.

[22] Innes, M., Edelman, A., Fischer, K., Rackauckus, C., Saba, E., Shah, V. B., and Tebbutt, W. (2019). Zygote: A differentiable programming system to bridge machine learning and scientific computing. *arXiv preprint arXiv:1907.07587*, page 140.

[23] Ioffe, S. and Szegedy, C. (2015). Batch normalization: Accelerating deep network training by reducing internal covariate shift. In *International conference on machine learning*, pages 448–456. PMLR.

[24] Izmailov, P., Vikram, S., Hoffman, M. D., and Wilson, A. G. (2021). What are bayesian neural network posteriors really like? *International Conference on Learning Representations*.

[25] Kelly, J., Bettencourt, J., Johnson, M. J., and Duvenaud, D. (2020). Learning differential equations that are easy to solve. In *Neural Information Processing Systems*.

[26] Kidger, P., Foster, J., Li, X., Oberhauser, H., and Lyons, T. (2021). Neural sdes as infinite-dimensional gans. *arXiv preprint arXiv:2102.03657*.

[27] Kidger, P., Morrill, J., Foster, J., and Lyons, T. (2020). Neural controlled differential equations for irregular time series. *arXiv preprint arXiv:2005.08926*.

[28] Kingma, D. P. and Ba, J. (2015). Adam: A method for stochastic optimization. *CoRR*, abs/1412.6980.

[29] Kong, L., Sun, J., and Zhang, C. (2020). Sde-net: Equipping deep neural networks with uncertainty estimates. *arXiv preprint arXiv:2008.10546*.

[30] Krizhevsky, A., Nair, V., and Hinton, G. (2014). The cifar-10 dataset. *online: http://www.cs.toronto.edu/kriz/cifar.html*, 55:5.

[31] Krueger, D., Huang, C.-W., Islam, R., Turner, R., Lacoste, A., and Courville, A. (2018). Bayesian hypernetworks. *arXiv preprint arXiv:1710.04759*.

[32] Li, X., Wong, T.-K. L., Chen, R. T., and Duvenaud, D. (2020). Scalable gradients for stochastic differential equations. *arXiv preprint arXiv:2001.01328*.

[33] Liu, X., Xiao, T., Si, S., Cao, Q., Kumar, S., and Hsieh, C.-J. (2019). Neural sde: Stabilizing neural ode networks with stochastic noise. *arXiv preprint arXiv:1906.02355*.

[34] Look, A. and Kandemir, M. (2019). Differential bayesian neural nets. *arXiv preprint arXiv:1912.00796*.

[35] Louizos, C. and Welling, M. (2017). Multiplicative normalizing flows for variational bayesian neural networks. In *Proceedings of the 34th International Conference on Machine Learning-Volume 70*, pages 2218–2227. JMLR. org.

[36] Mishkin, A., Kunstner, F., Nielsen, D., Schmidt, M., and Khan, M. E. (2018). Slang: Fast structured covariance approximations for bayesian deep learning with natural gradient. In *Advances in Neural Information Processing Systems*, pages 6245–6255.

[37] Neal, R. M. (1996). *Bayesian learning for neural networks*, volume 118. Springer Science & Business Media.

[38] Oganesyan, V., Volokhova, A., and Vetrov, D. (2020). Stochasticity in neural odes: An empirical study. *arXiv preprint arXiv:2002.09779*.

[39] Opper, M. (2019). Variational inference for stochastic differential equations. *Annalen der Physik*, 531(3):1800233.

[40] Osawa, K., Swaroop, S., Jain, A., Eschenhagen, R., Turner, R. E., Yokota, R., and Khan, M. E. (2019). Practical deep learning with bayesian principles. *arXiv preprint arXiv:1906.02506*.

[41] Peluchetti, S. and Favaro, S. (2020a). Doubly infinite residual networks: a diffusion process approach.

[42] Peluchetti, S. and Favaro, S. (2020b). Infinitely deep neural networks as diffusion processes. In *International Conference on Artificial Intelligence and Statistics*, pages 1126–1136. PMLR.

[43] Rezende, D. J., Mohamed, S., and Wierstra, D. (2014). Stochastic backpropagation and approximate inference in deep generative models. *arXiv preprint arXiv:1401.4082*.

[44] Roeder, G., Wu, Y., and Duvenaud, D. K. (2017). Sticking the landing: Simple, lower-variance gradient estimators for variational inference. In *Advances in Neural Information Processing Systems*, pages 6925–6934.

[45] Rubanova, Y., Chen, R. T. Q., and Duvenaud, D. (2019). Latent odes for irregularly-sampled time series. *arXiv preprint arXiv:1907.03907*.

[46] Ryder, T., Golightly, A., McGough, A. S., and Prangle, D. (2018). Black-box variational inference for stochastic differential equations. In *International Conference on Machine Learning*, pages 4423–4432. PMLR.

[47] Tzen, B. and Raginsky, M. (2019a). Neural stochastic differential equations: Deep latent gaussian models in the diffusion limit. *arXiv preprint arXiv:1905.09883*.

[48] Tzen, B. and Raginsky, M. (2019b). Theoretical guarantees for sampling and inference in generative models with latent diffusions. *arXiv preprint arXiv:1903.01608*.

[49] Wang, K.-C., Vicol, P., Lucas, J., Gu, L., Grosse, R., and Zemel, R. (2018). Adversarial distillation of bayesian neural network posteriors. *arXiv preprint arXiv:1806.10317*.

[50] Wenzel, F., Roth, K., Veeling, B., Swiatkowski, J., Tran, L., Mandt, S., Snoek, J., Salimans, T., Jenatton, R., and Nowozin, S. (2020). How good is the bayes posterior in deep neural networks really? In *International Conference on Machine Learning*, pages 10248–10259. PMLR.

[51] Yıldız, Ç., Heinonen, M., and Lähdesmäki, H. (2019). Ode<sup>2</sup>vae: Deep generative second order odes with bayesian neural networks. *arXiv preprint arXiv:1905.10994*.

[52] Zadrozny, B. and Elkan, C. (2002). Transforming classifier scores into accurate multiclass probability estimates. In *Proceedings of the Eighth ACM SIGKDD International Conference on Knowledge Discovery and Data Mining*, page 694–699.

[53] Zhang, G., Sun, S., Duvenaud, D., and Grosse, R. (2018). Noisy natural gradient as variational inference. In *International Conference on Machine Learning*, pages 5852–5861.

[54] Zhang, H., Dauphin, Y. N., and Ma, T. (2019a). Fixup initialization: Residual learning without normalization. *arXiv preprint arXiv:1901.09321*.

[55] Zhang, H., Gao, X., Unterman, J., and Arodz, T. (2019b). Approximation capabilities of neural ordinary differential equations. *arXiv preprint arXiv:1907.12998*.

[56] Zhang, T., Yao, Z., Gholami, A., Keutzer, K., Gonzalez, J., Biros, G., and Mahoney, M. W. (2019c). ANODEV2: A coupled neural ODE evolution framework. *CoRR*, abs/1906.04596.

## A Appendix

**Notation.** Denote as  $\phi$  the vector of variational parameters,  $f_q$  as the approximate posterior on weights,  $f_p$  as the prior on weights,  $f_h$  as the dynamics of hidden units, and  $\sigma$  as the diffusion function. Denote the Euclidean norm of a vector  $u$  by  $|u|$ . For function  $f$  denote its Jacobian as  $\nabla f$ .

### A.1 Derivation of an Alternative Monte Carlo Estimator

The goal of this section is to derive a Monte Carlo estimator of the KL-divergence on path space that is similar to the *fully Monte Carlo* estimator described in [44]. This will serve as the basis for the subsequent heuristic derivation of the continuous-time sticking-the-landing trick.

Let  $w_0$  be a fixed initial state. Let  $w_1, \dots, w_N$  be states at times  $\Delta t, 2\Delta t, \dots, N\Delta t = T$  generated by the Euler discretization:

$$w_{i+1} = w_i + f_q(w_i)\Delta t + \sigma(w_i)(B_{t+\Delta t} - B_t) \quad (13)$$

$$= w_i + f_q(w_i)\Delta t + \sigma(w_i)\Delta t^{1/2}\epsilon_{i+1}, \quad \epsilon_{i+1} \sim \mathcal{N}(0, 1). \quad (14)$$

where  $\{B_t\}_{t \geq 0}$  is the Brownian motion. This implies that conditional on the previous state, the current state is normally distributed:

$$w_{i+1}|w_i \sim \mathcal{N}(w_i + f_q(w_i)\Delta t, \sigma(w_i)^2\Delta t).$$

Thus, the log-densities can be evaluated as

$$\log q(w_{i+1}|w_i) = -\frac{1}{2} \log(2\pi\sigma(w_i)^2\Delta t) - \frac{1}{2} \frac{(w_{i+1} - (w_i + f_q(w_i)\Delta t))^2}{\sigma(w_i)^2\Delta t}, \quad i = 0, \dots, N-1. \quad (15)$$

On the other hand, if at any time, the next state was generated from the current state based on the prior process, we would have the following log-densities:

$$\log p(w_{i+1}|w_i) = -\frac{1}{2} \log(2\pi\sigma(w_i)^2\Delta t) - \frac{1}{2} \frac{(w_{i+1} - (w_i + f_p(w_i)\Delta t))^2}{\sigma(w_i)^2\Delta t}, \quad i = 0, \dots, N-1. \quad (16)$$

Now, we substitute the form of  $w_{i+1}$  based on equation 13 into equation 15 and equation 16 and obtain

$$\begin{aligned} \log q(w_{i+1}|w_i) &= -\frac{1}{2} \log(2\pi\sigma(w_i)^2\Delta t) - \frac{1}{2}\epsilon_{i+1}^2, \\ \log p(w_{i+1}|w_i) &= -\frac{1}{2} \log(2\pi\sigma(w_i)^2\Delta t) \\ &\quad - \frac{1}{2} \left( \frac{(f_q(w_i) - f_p(w_i))^2}{\sigma(w_i)^2} \Delta t + \frac{2(f_q(w_i) - f_p(w_i))\epsilon_{i+1}}{\sigma(w_i)} \Delta t^{1/2} + \epsilon_{i+1}^2 \right). \end{aligned}$$

The KL divergence on the path space could then be regarded as a sum of infinitely many KL-divergences between Gaussians:

$$\lim_{N \rightarrow \infty} \sum_{i=0}^N \mathbb{E}_{w_i} [D_{\text{KL}}(q(w_{i+1}|w_i) || p(w_{i+1}|w_i))] \quad (17)$$

$$= \lim_{N \rightarrow \infty} \sum_{i=0}^N \mathbb{E}_{w_i} \left[ \mathbb{E}_{w_{i+1} \sim q(w_{i+1}|w_i)} \left[ \log \frac{q(w_{i+1}|w_i)}{p(w_{i+1}|w_i)} \right] \right] \quad (18)$$

$$= \lim_{N \rightarrow \infty} \sum_{i=0}^N \mathbb{E}_{w_i} \left[ \mathbb{E}_{\epsilon_{i+1}} \left[ \frac{(f_q(w_i) - f_p(w_i))^2}{2\sigma(w_i)^2} \Delta t + \frac{(f_q(w_i) - f_p(w_i))}{\sigma(w_i)} \Delta t^{1/2} \epsilon_{i+1} \right] \right] \quad (19)$$

$$= \mathbb{E} \left[ \frac{1}{2} \int_0^T |u_t|^2 dt + \int_0^T u_t dB_t \right]. \quad (20)$$

## A.2 Sticking-the-landing in Continuous Time

For a non-sequential latent variable model, the sticking-the-landing (STL) trick removes from the fully Monte Carlo ELBO estimator a score function term of the form  $\partial \log q(w, \phi) / \partial \phi$ , where  $w$  is sampled using the reparameterization trick and may depend on  $\phi$ . The score function term has 0 expectation, but may affect the variance of the gradient estimator for the inference distribution's parameters.

Here, we exploit this intuition and apply it to each step before taking the limit. More precisely, we apply the STL trick to estimate the gradient of  $D_{\text{KL}}(q(w_{i+1}|w_i) || p(w_{i+1}|w_i))$  for  $i = 1, 2, \dots, N$ , and thereafter take the limit as the mesh size of the discretization goes to 0. For each individual term, the score function term to be removed is

$$\begin{aligned}\frac{\partial}{\partial \phi} \log q(w_{i+1}|w_i, \phi) &= -\frac{1}{2\sigma^2(w_i)\Delta t} \frac{\partial}{\partial \phi} \left[ (w_{i+1} - (w_i + f_q(w_i, \phi)\Delta t))^2 \right] \\ &= \frac{\partial}{\partial \phi} \left[ \frac{f_q(w_i, \phi)}{\sigma(w_i)} \right] \epsilon_{i+1} \Delta t^{1/2}.\end{aligned}$$

Now, we sum up all of these terms and take the limit as  $\Delta t \rightarrow 0$ . This gives us

$$\begin{aligned}&\lim_{N \rightarrow \infty} \sum_{i=0}^N \mathbb{E}_{w_i} \left[ \mathbb{E}_{w_{i+1} \sim q(w_{i+1}|w_i)} \left[ \frac{\partial}{\partial \phi} \log q(w_{i+1}|w_i) \right] \right] \\ &= \lim_{N \rightarrow \infty} \sum_{i=0}^N \mathbb{E}_{w_i} \left[ \mathbb{E}_{\epsilon_{i+1}} \left[ \frac{\partial}{\partial \phi} \left[ \frac{f_q(w_i, \phi)}{\sigma(w_i)} \right] \epsilon_{i+1} \Delta t^{1/2} \right] \right] \\ &= \mathbb{E} \left[ \int_0^T \frac{\partial}{\partial \phi} \left[ \frac{f_q(w_t, \phi)}{\sigma(w_t)} \right] dB_t \right] \\ &= \mathbb{E} \left[ \int_0^T \frac{\partial}{\partial \phi} [u_t] dB_t \right].\end{aligned}$$

Removing this term from the fully Monte Carlo estimator in equation 20 gives rise to the following estimator of a surrogate objective that facilitates implementation:

$$\begin{aligned}\widehat{\text{ELBO}} &= \log p(\mathcal{D} | w) - \int_{t_0}^{t_1} \frac{1}{2} \|u(w_t, t, \phi)\|_2^2 dt \\ &\quad - \int_{t_0}^{t_1} u(w_t, t, \text{stop\_gradient}(\phi)) dB_t, \quad w(\cdot) \sim q_\phi().\end{aligned}$$

### A.3 Additional Results

#### A.3.1 Augmentation in Differential Equation Models

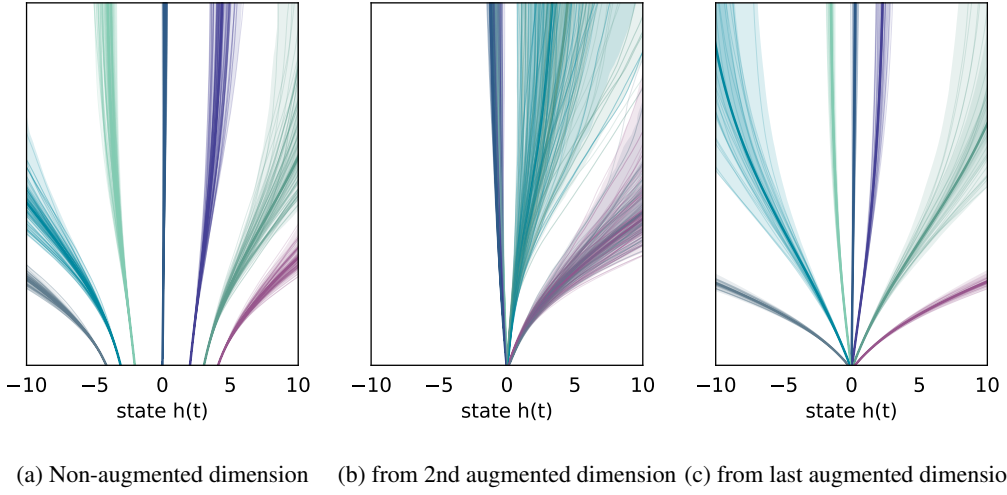


Figure 8: Example flows sampled from learned SDE dynamics. All continuous-depth models were trained by augmenting the state by 2 dimensions, refer to Figure 1 for main results. *Left:* The SDE-BNN learns meaningful parameterizations on the non-extraneous dimensions of the input state vector. In the case of a true function being monotonic, the augmented dimensions simply help the main output. *Middle:* The model learns to ignore dimensions that are not necessary to train on, especially on simpler tasks as in the toy setting. Samples in augmented dimensions can overlap for different input values in the given domain  $(-5, 5)$ . *Right:* Similarly, the last output dimension was also associated with augmentation and was not a well learned representation of the data, ignoring the initial inputs entirely (all values are 0).

Table 2: These are the hyper-parameters for each method of evaluation pertaining to results in the toy and classification tasks of Table 1. Each model was run on a single Nvidia RTX6000 GPU on our compute clusters. SDE and learning optimization parameters were tuned according to a validation set sampled randomly from 10% of the training set. No schedules of any kind on the hyper-parameters were used in training. Settings with high overlap with another model are indicated using  $\langle \text{model} \rangle$  with additional parameters overridden as necessary. Each block is separated either by a downsampling or upsampling convolutional layer (i.e., the  $'$ s).

| Model            | Hyper-parameter                      | EXPERIMENTS                      |                                      |                                      |
|------------------|--------------------------------------|----------------------------------|--------------------------------------|--------------------------------------|
|                  |                                      | 1D Regression                    | MNIST [9]                            | CIFAR-10 [30]                        |
| ResNet32         | Learning Rate                        | –                                | 1e-3                                 | 7e-4                                 |
|                  | Batch Size                           | –                                | 128                                  | 128                                  |
|                  | Activation                           | –                                | tanh                                 | tanh                                 |
|                  | Epochs                               | –                                | 100                                  | 500                                  |
| ODEnet           | Augment dim.                         | 2                                | 2                                    | 2                                    |
|                  | # blocks                             | 1                                | 1                                    | 2-2-2                                |
|                  | Diffusion $\sigma$                   | 0                                | 0                                    | 0                                    |
|                  | KL coef.                             | 0                                | 0                                    | 0                                    |
|                  | Learning Rate                        | 1e-3                             | 1e-3                                 | 7e-4                                 |
|                  | # Solver Steps                       | 10                               | 20                                   | 20                                   |
|                  | Batch Size                           | 40                               | 128                                  | 128                                  |
|                  | Activation                           | swish                            | tanh                                 | tanh                                 |
|                  | Epochs                               | 800                              | 100                                  | 500                                  |
| HyperODEnet      | $\langle \text{ODEnet} \rangle$      | –                                | $\langle \text{ODEnet} \rangle$      | $\langle \text{ODEnet} \rangle$      |
|                  | KL coef.                             | –                                | 1e-3                                 | 1e-3                                 |
|                  | Drift $f_w$ dim.                     | –                                | 1-64-1                               | 1-128-1                              |
| MFVI ResNet32    | $\langle \text{ResNet32} \rangle$    | –                                | $\langle \text{ResNet32} \rangle$    | $\langle \text{ResNet32} \rangle$    |
|                  | KL coef.                             | –                                | 1e-3                                 | 1e-3                                 |
| MFVI ODEnet      | $\langle \text{ODEnet} \rangle$      | –                                | $\langle \text{ODEnet} \rangle$      | $\langle \text{ODEnet} \rangle$      |
|                  | KL coef.                             | –                                | 1e-3                                 | 1e-3                                 |
| MFVI HyperODEnet | $\langle \text{MFVI ODEnet} \rangle$ | –                                | $\langle \text{MFVI ODEnet} \rangle$ | $\langle \text{MFVI ODEnet} \rangle$ |
|                  | Drift $f_w$ dim.                     | –                                | 1-64-1                               | 1-128-1                              |
| SDE BNN          | $\langle \text{ODEnet} \rangle$      | $\langle \text{ODEnet} \rangle$  | $\langle \text{ODEnet} \rangle$      | $\langle \text{ODEnet} \rangle$      |
|                  | Learning Rate                        | 1e-3                             | 1e-3                                 | 7e-4                                 |
|                  | # blocks                             | 1                                | 1                                    | 2-2-2                                |
|                  | Drift $f_x$ dim.                     | 32                               | 32                                   | 64                                   |
|                  | Drift $f_w$ dim.                     | 32                               | 1-64-1                               | 2-128-2                              |
|                  | Diffusion $\sigma$                   | 0.2                              | 0.1                                  | 0.1                                  |
|                  | # Posterior Samples                  | 20                               | 1                                    | 1                                    |
| SDE BNN (+ STL)  | $\langle \text{SDE BNN} \rangle$     | $\langle \text{SDE BNN} \rangle$ | $\langle \text{SDE BNN} \rangle$     | $\langle \text{SDE BNN} \rangle$     |

Table 3: Classification accuracy and expected calibration error on MNIST (100<sup>th</sup> epoch) and CIFAR-10 (300<sup>th</sup> epoch) for additional baseline to the ones in Table 1. Values are compared at the 100th epoch for MNIST and 300th for CIFAR-10. Here  $w_0$ , the initial drift of the posterior SDE, is inferred using a Gaussian prior rather than being a fixed value. The best prior variance was selected in a preliminary sweep between values in the range [0.1, 0.44]. The performance is slightly worse than the point estimate but displays better calibration as a trade-off. It can be noted that calibration may appear better earlier on in training, as in prior to converging and reaching non-uniform confidence, but model predictions are not necessarily correct.

| Model                          | MNIST            |                          | CIFAR-10         |                          |
|--------------------------------|------------------|--------------------------|------------------|--------------------------|
|                                | Accuracy (%)     | ECE ( $\times 10^{-2}$ ) | Accuracy (%)     | ECE ( $\times 10^{-2}$ ) |
| SDE BNN                        | $99.30 \pm 0.09$ | $0.63 \pm 0.10$          | $88.08 \pm 1.25$ | $7.53 \pm 0.44$          |
| SDE BNN (+ STL)                | $99.10 \pm 0.09$ | $0.78 \pm 0.12$          | $87.95 \pm 1.32$ | $7.94 \pm 0.59$          |
| SDE BNN $w_0$ inferred         | $99.04 \pm 0.03$ | $0.73 \pm 0.04$          | $88.04 \pm 0.30$ | $6.56 \pm 0.62$          |
| SDE BNN $w_0$ inferred (+ STL) | $99.05 \pm 0.00$ | $0.79 \pm 0.04$          | $87.37 \pm 0.63$ | $6.44 \pm 0.10$          |

Table 4: Training with STL estimator shows improvements on training accuracy, negative log likelihood, and ELBO objective in addition to reducing variance. In settings where the approximate posterior is sufficiently flexible (i.e. the drift neural net is very large relative to the state size), it can outperform the standard gradient estimator.

| Method         | Accuracy (%)    | Negative Log-likelihood ( $\times 10^{-4}$ ) | ELBO            |
|----------------|-----------------|--|-----------------|
| SDE BNN        | $95.91 \pm 0.2$ | $1.17 \pm 0.309$                             | $1.40 \pm 0.2$  |
| SDE BNN (+STL) | $96.89 \pm 0.2$ | $0.309 \pm 0.15$                             | $1.183 \pm 0.2$ |

Table 5: Properties of various Bayesian supervised learning approaches.

| Method               | Posterior over Stochastic Process | Flexible Approximate Posterior | Adaptive Computation | References                          |
|----------------------|-----------------------------------|--------------------------------|----------------------|-------------------------------------|
| Bayes by Backprop    | ✗                                 | ✗                              | ✗                    | Blundell et al. [3]                 |
| MCMC for BNNs        | ✗                                 | ✓                              | ✗                    | e.g. [37, 50, 24]                   |
| Bayesian Hypernets   | ✗                                 | ✓                              | ✗                    | Krueger et al. [31]                 |
| BBVI for SDEs        | ✓                                 | ✗                              | ✗                    | Ryder et al. [46]                   |
| Bayesian Neural ODEs | ✗                                 | ✗                              | ✓                    | Yildiz et al. [51]                  |
| SDE-BNN              | ✓                                 | ✓                              | ✓                    | Dandekar et al. [7]<br>current work |

### A.3.2 Calibration

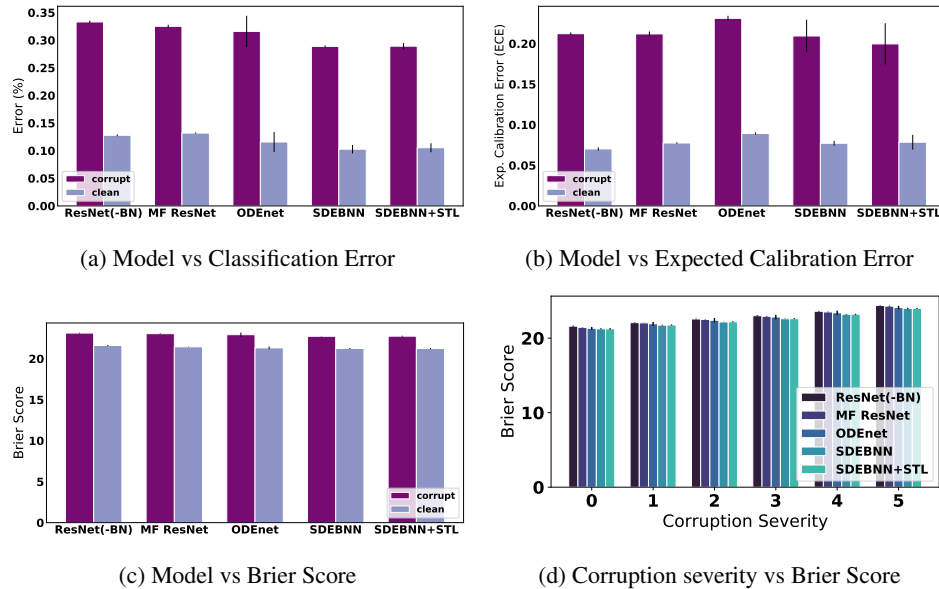


Figure 9: Figures 9a-9c show that the SDE BNN and SDE BNN + STL models outperform their non-continuous depth ResNet counterparts on all three robustness metrics when evaluated on the corrupt CIFAR-10C benchmarks. Figure 9d indicates that the accuracy of predictions is relatively consistent across all severity levels with the SDE-BNN and SDE-BNN + STL models having relatively better calibrated predictions.

### A.3.3 Comparisons with Other Bayesian Models

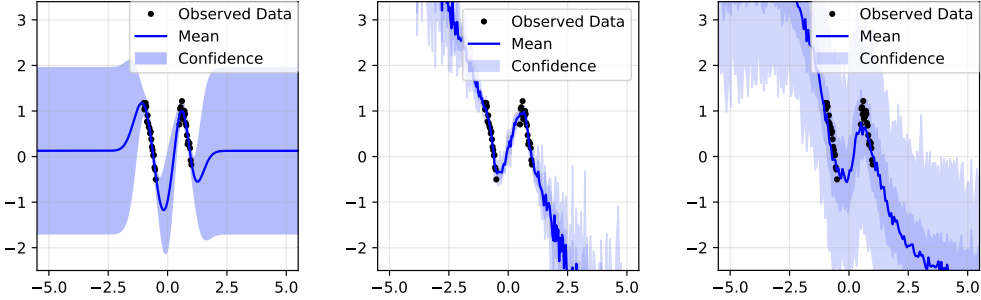


Figure 10: Approximate posteriors from other common Bayesian statistical models. Left: Gaussian Process. Center: Deep Ensemble K=8. Right: MFVI. Different variances and extrapolations are learned from the SDE-BNN across other Bayesian model parameterizations, which can result in more or less reasonable uncertainty bounds depending on interpretation.

### A.3.4 Robustness to solver error at test time

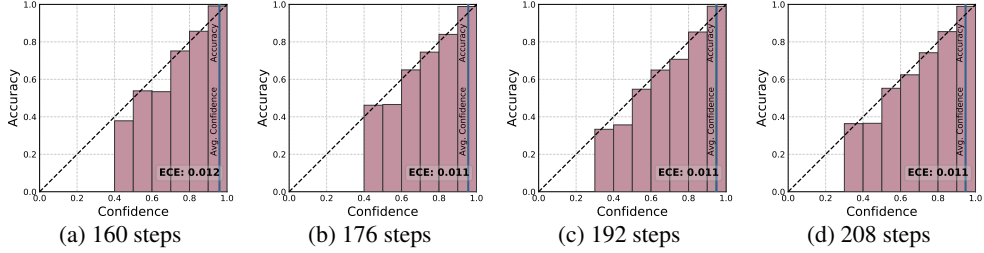


Figure 11: CIFAR10 image classification with a SDE-BNN. Better calibration can be obtained by increasing solver step sizes during inference without substantially changing the training error.

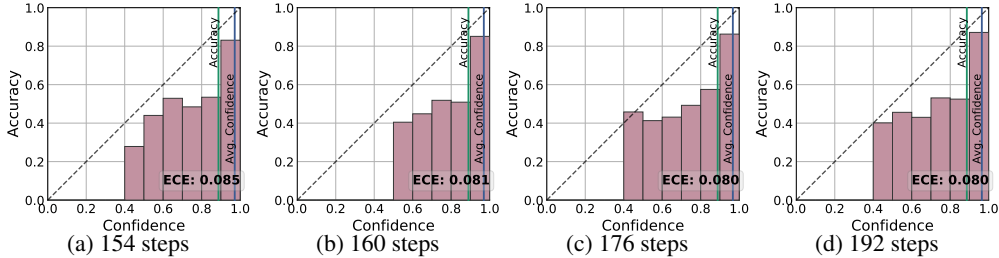


Figure 12: CIFAR10 image classification with a SDE-BNN. Generalization improves marginally compared to a trained model during inference in 12b, as tuning solver step size does not yield significant differences in calibration outcomes.

### A.3.5 Different SDE solver and adjoint settings

These were run with a SDE-BNN for MNIST image classification, to compare the performance and run-time cost across different solver settings. Comparably, backpropagation through the solver averaged 162.58 sec / epoch while the adjoint method averaged 135.90 sec / epoch in terms of wall clock time.

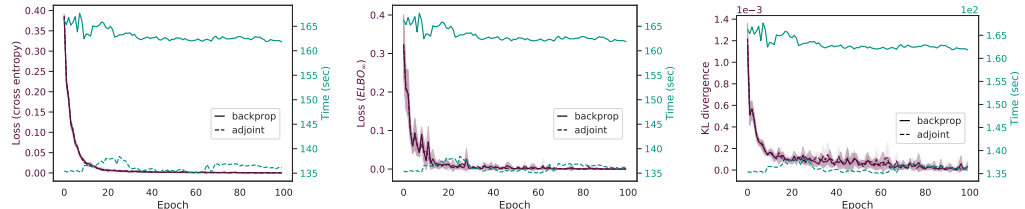


Figure 13: Backpropagation through the SDE solver yields similar optimization dynamics but is less time efficient than the adjoint method.

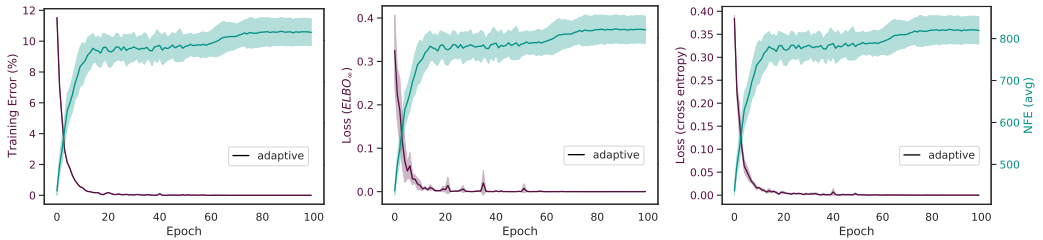


Figure 14: Trade-off between solver speed and convergence during training. Adaptive refers to training with the stochastic adjoint in both forward and reverse modes here.

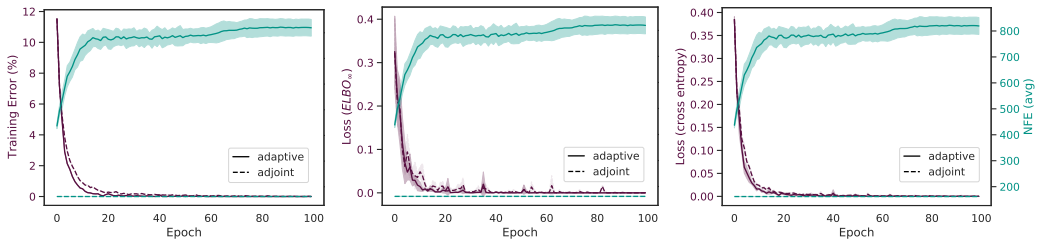


Figure 15: Trade-off between solver speed and precision during training. Adaptive-order optimization trajectories were comparable to fixed-order solvers and were thus not applied to the classification tasks since computational resources were not under constraint.